Numerical pore-scale modeling of three-phase fluid flow: Comparison between simulation and experiment

G. G. Pereira*
Australian Petroleum Cooperative Research Centre, University of New South Wales, Sydney 2052, Australia
(Received 4 May 1998; revised manuscript received 25 August 1998)

It has been recently shown experimentally by Øren and Pinczewski [SPE Form. Eval. **7**, 70 (1992); **9**, 149 (1994)] that on the pore scale the presence of continuous wetting and spreading films is vitally important in describing the mobility of the various fluid phases in three-phase fluid flow. In this paper we put in place a numerical, pore-scale model to describe three-phase drainage dominated flow. Our model incorporates all the mechanisms observed in glass micromodel experiments. The pressures of all phases are calculated explicitly so that no *ad hoc* rules need be introduced to describe fluid flow. In doing this we are able to reproduce many of the experimentally observed characteristics of three-phase flow, i.e., multiple, simultaneous displacements, flow through thin wetting and spreading films, and double drainage events. The numerical simulations are carried out for a variety of wetting and spreading conditions, i.e., oil-wet, water-wet, positive spreading, and negative spreading, and in all cases we see good agreement with micromodel experiments.
[S1063-651X(99)12703-X]

PACS number(s): 47.55.Mh, 64.60.Ak

I. INTRODUCTION

An improved oil recovery process that is becoming increasingly important is that of immiscible gas flooding to recover water-flood residual oil. There is now a growing body of work devoted to understanding the basic three-phase gas-oil-water displacement mechanisms responsible for the mobilization of water-flood residual oil. An understanding of these processes is necessary for the prediction of the phase permeabilities in regions of the reservoir where oil, water, and gas flow simultaneously.

A description of *two-phase* fluid flow in porous media is well understood, with the macroscopic properties of fluid flow described in terms of Darcy's law and experimentally determined saturation dependent relationships for phase relative permeabilities and capillary pressures. On the other hand, an analogous description of *three-phase* fluid flow is not well understood. The primary problem is that the corresponding experiments for three-phase flow are not only difficult to carry out but also particularly hard to interpret, e.g., see Honarpour, Koederitz, and Harvey [1], and references therein.

In practice macroscopic three-phase fluid flow relationships are determined using estimates from two-phase flow data. The most commonly used models are those due to Stone [2,3] and variations of this basic model (e.g., see Fayers and Matthews [4], Parker and Lenhard [5], and Aleman and Slattery [6]). Comparisons of results between these simplistic models and experimental measurements are contradictory [4,7–9]. This is not surprising since, in principle, the extra third phase, which in the rest of this paper will be called the intermediate phase, has properties unlike the other two phases (i.e., the wetting and nonwetting phases).

Recent work concerned with pore-scale mechanisms by Kantzas, Chatzis, and Dullien [10], Øren and co-workers [11–14], Kalaydjian *et al.* [15], and Blunt, Fenwick, and Zhou [16] has clearly demonstrated the importance of flow through intermediate phase spreading films in determining phase mobilities and fluid trapping in three-phase flow. Spreading is a three-phase phenomenon which is not accounted for in these predictive models. These spreading films allow the intermediate phase to be mobile even at extremely low saturations, in direct contrast to the commonly used predictive models [2–4].

In principle, it is not necessary to actually measure two-phase or three-phase relative permeability and capillary pressure data since it is possible to determine these by appropriately averaging the equations describing the physical processes occurring on the microscopic or pore scale. This approach requires a detailed understanding of displacement mechanisms on the pore scale and a complete description of the morphology of the pore space. The procedure has been applied, with success, to two-phase flow using pore-scale physics identified in micromodel experiments [17] with the morphology of the pore space represented by a topologically equivalent numerical network. The studies by Blunt and King [18], Blunt, King, and Scher [19], and Jerauld and Salter [20] are good examples of the success of this approach. Although the difficulty in adequately describing the complex morphology of the pore space for actual porous media has limited this approach to idealized porous media, network models have proved to be powerful tools for developing important insights into complex two-phase flow phenomena (hysteresis, trapping, film flow—see references already cited) and for extrapolating limited measured data. Moreover, for three-phase flow, network models offer the possibility of overcoming the serious experimental difficulties encountered in measuring three-phase relative permeabilities and of providing data under strictly controlled conditions which will be necessary for the development of

*Present address: Department of Applied Mathematics, Research School of Physical Sciences and Engineering, Australian National University, Canberra 0200, ACT, Australia.

improved methods for predicting relative permeabilities in three-phase flow, see Heiba, Davis, and Scriven [21].

The application of network modeling techniques to three-phase flow is considerably less developed than for two-phase flow and no models currently exist which can realistically predict the effects of both viscous and capillary forces on three-phase displacements. Heiba, Davis, and Scriven [21] used percolation concepts to model three-phase flow in porous media. Fenwick and Blunt [22] extended the model to three dimensions. Soll and Celia [23] and Øren and Pinczewski [14] modified the percolation algorithms to approximate the effects of film flow. None of the previous models provide a rigorous treatment of flow through both wetting and spreading films. The algorithms therefore require *ad hoc* estimates of the viscous pressure drops associated with film flow and the introduction of trapping rules in order to match measured fluid recoveries.

The purpose of the present paper is to present a two-dimensional network model for drainage dominated three-phase flow, in both water-wet and oil-wet porous media, where both capillary and viscous effects are important. The model is based on the pore-scale displacement mechanisms described by Øren and co-workers [11–14]. By solving the pressure equations in the three fluid phases no extraneous rules need to be added to account for viscous pressure drops. Computed fluid recoveries are compared with the two-dimensional glass micromodel displacement experiments reported by Øren, Billiote, and Pinczewski [11]. The comparison shows that the model provides a correct macroscopic description of the displacement process. Differences in recoveries for the various cases studied are fully accounted for by the present network model. This confirms the validity of the pore-scale displacement mechanisms on which the model is based and provides a basis for extending three-phase network models to three dimensions.

II. PORE-SCALE FLUID DISTRIBUTION

A pore-scale description of three-phase fluid flow has been provided in detail by Øren and co-workers [11–13]. Here we briefly introduce those concepts that are necessary for defining our network model.

When a porous medium is occupied by three immiscible fluids, the ease with which a fluid can flow in response to a pressure gradient is determined by the distribution and connectivity of the fluids in the pore space. Øren and Pinczewski [14] showed that when one of the fluids completely wets the solid, the equilibrium distribution of the fluids depends on *wettability*, *capillary pressure*, and the *spreading behavior* of the fluids. Following the description of Øren and Pinczewski [14], we designate the fluids as fluid 1, fluid 2, and fluid 3, with fluid 3 being the wetting fluid.

The three-phase gas-oil-water displacements carried out by Øren and co-workers [11–13] were carried out in glass micromodels under strongly water-wet and strongly oil-wet conditions with fluids displaying positive and negative spreading behavior. The spreading behavior refers to oil spreading on water in the presence of air and is determined by the equation which defines the initial oil-water spreading coefficient S_{ow},

$$S_{ow}=\sigma_{gw}-\sigma_{go}-\sigma_{ow}, \tag{1}$$

TABLE I. Measured interfacial tensions for experimental systems according to Øren, Billiote, and Pinczewski [11].

	σ_{gw}	σ_{og}	σ_{ow}
Positive spreading system	73.3	23.0	32.6
Negative spreading system	33.1	20.9	20.3

where σ is the interfacial tension and the subscripts g, w, and o denote gas, water, and oil, respectively. If $S_{ow}>0$, oil spreads on the water surface while if $S_{ow}<0$ it does not. The measured interfacial tensions for the experimental fluid systems are given in Table I. For these interfacial tensions the fluid distribution in the pore space may be categorized into four separate cases as shown in Fig. 1. Figures 1(a) and 1(b) show the distribution for the water-wet case while Figs. 1(c) and 1(d) show the distribution for the oil-wet case.

Capillary pressures dictate that the wetting fluid is preferentially located in the smaller pore throats and it forms continuous wetting films which hydraulically connect the wetting fluid throughout the entire medium.

For the case of three fluids in a porous medium, there are two nonwetting fluids (fluid 1 and fluid 2). In Figs. 1(a) and 1(b), gas and oil are the nonwetting fluids while in Figs. 1(c) and 1(d) gas and water are the nonwetting fluids.

In regions of the pore space occupied by all three fluids, the two nonwetting fluids may compete to occupy the same pore body. The fluid which preferentially occupies the pore

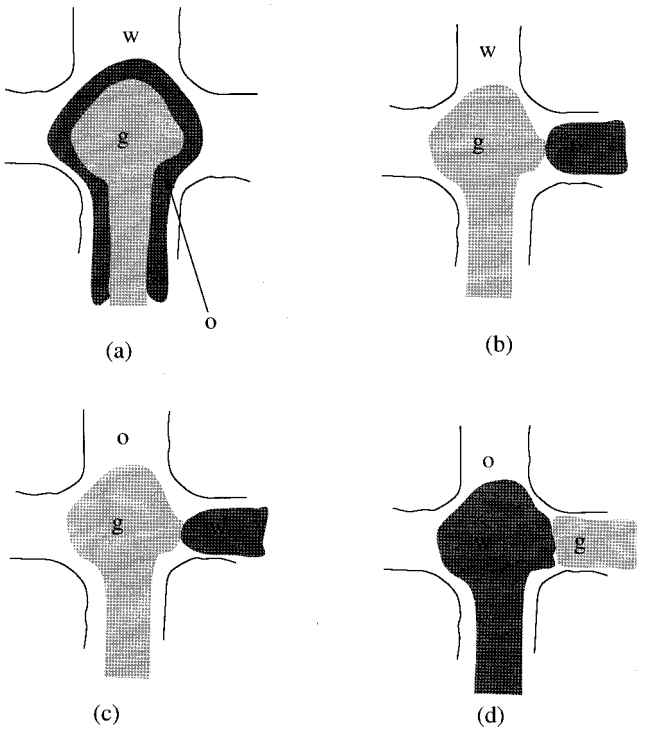

FIG. 1. Three-phase fluid distribution in glass micromodel experiments of Øren and co-workers. (a) Strongly water-wet conditions with a positive spreading coefficient (gas 1, oil 2, water 3), (b) strongly water-wet conditions with a negative spreading coefficient (gas 1, oil 2, water 3), (c) strongly oil-wet conditions with a negative spreading coefficient (gas 1, water 2, oil 3), and (d) strongly oil-wet conditions with a positive spreading coefficient (water 1, gas 2, oil 3). Note in (d) the interchange in roles of water and gas.

body is the one having the greater capillary pressure with the wetting fluid, i.e., the more strongly nonwetting fluid. For strongly wetting conditions, this will be fluid 1 when

$$\sigma_{13} > \sigma_{23}, \tag{2}$$

where σ_{13} and σ_{23} are the fluid-1–fluid-3 and fluid-2–fluid-3 interfacial tensions, respectively. When condition (2) is satisfied, we refer to fluid 1 as the *nonwetting fluid* and fluid 2 as the *intermediate fluid*. Table I shows that for the water-wet systems being considered, gas is the nonwetting fluid (fluid 1 is *gas*) and oil is the intermediate fluid (fluid 2 is *oil*), since $\sigma_{gw} > \sigma_{ow}$ for both systems. For the oil-wet, negative spreading system, gas is the nonwetting fluid (fluid 1 is *gas*) and water is the intermediate fluid (fluid 2 is *water*). However, for the oil-wet, positive spreading system water is the nonwetting fluid (fluid 1 is *water*) and gas is the intermediate fluid (fluid 2 is *gas*), since $\sigma_{wo} > \sigma_{go}$.

The manner in which the intermediate fluid is distributed depends on the fluid-2–fluid-3 spreading coefficient S_{23}, which is defined as

$$S_{23} = \sigma_{13} - \sigma_{23} - \sigma_{12}. \tag{3}$$

S_{23} is the initial spreading coefficient measured on pure fluids before they are brought into contact with each other. A final spreading coefficient, S_{23}^e, is measured when the fluids are in thermodynamic equilibrium. Although S_{23} may be positive or negative, S_{23}^e is either zero or negative [24,25]. Once thermodynamic equilibrium has been established, the fluids may adopt one of three basic configurations depending on the value of S_{23}^e.

(i) If $S_{23}^e = 0$, the intermediate fluid spontaneously spreads between the nonwetting and wetting fluids to form a thin, continuous spreading film which everywhere separates the two fluids, i.e., the intermediate fluid completely wets the nonwetting fluid. The thin molecular film of intermediate fluid which initially spreads between the wetting and nonwetting fluids first swells and is then stabilized by capillary forces in the corners of the pore space [16]. This is the case for the water-wet positive spreading system as shown in Fig. 1(a).

(ii) If $-2\sigma_{12} < S_{23}^e < 0$, the intermediate fluid does not spread and the nonwetting and wetting fluids are separated by a three-phase contact line, i.e., the intermediate fluid only partially wets the nonwetting fluid. If we assume the interfaces to be approximately planar, the contact angle at the nonwetting–intermediate fluid interface, θ_{12}, may be estimated from the Young equation

$$\cos\theta_{12} = 1 + \frac{S_{23}^e}{\sigma_{12}}. \tag{4}$$

This is the case for the water-wet negative spreading system, Fig. 1(b), as well as the oil-wet negative spreading system, Fig. 1(c).

Recently, it has been shown, both experimentally [26] and theoretically [16,22,26], that stable intermediate fluid films can be formed in the corners of angular pores over a limited range of capillary pressures under negative spreading conditions. For strongly wetting conditions, the criterion which must be satisfied for this to occur may be approximated from a capillary pressure analysis and is given by [22]

$$\frac{r_{23}}{r_{12}} < 1 + \frac{S_{23}^e}{\sigma_{12}} - \tan\beta\left[-\frac{S_{23}^e}{\sigma_{12}}\left(2 + \frac{S_{23}^e}{\sigma_{12}}\right)\right]^{1/2}, \tag{5}$$

where β is the corner half angle and r_{23} and r_{12} are the mean radii of curvature for the fluid-2–fluid-3 and fluid-1–fluid-2 interfaces, respectively. Condition (5) shows that the range of capillary pressures where stable intermediate fluid films exist decreases as the spreading coefficient becomes more negative. Condition (5) is never satisfied for the experimental conditions and fluid systems shown in Fig. 1.

(iii) When $S_{23}^e < -2\sigma_{12}$, a stable contact angle cannot exist and fluid 3 spontaneously spreads between the nonwetting and intermediate fluids to form a thin film which everywhere separates the two fluids. The thin spreading film is in hydraulic communication with the thicker wetting film covering the solid surface. This is the case for the oil-wet positive spreading system, Fig. 1(d). The physical situation is similar to that which exists for the case when the three fluids meet in a contact line and the connectivity of the fluids is also similar for the two cases [compare with Figs. 1(b) and 1(c)].

For the water-wet systems being considered, the most important difference between the fluid distributions shown in Figs. 1(a) and 1(b) is the connectivity of the intermediate fluid. For the positive spreading system, intermediate fluid (oil) spreading films hydraulically connect the intermediate fluid in a manner exactly analogous to that of wetting films connecting the wetting fluid. The spreading films allow the intermediate fluid to retain mobility down to very low intermediate phase saturations. For negative spreading systems, there are no spreading films and the intermediate fluid remains largely disconnected.

The most important difference between the fluid distributions for the two oil-wet systems being considered is the interchange of the nonwetting and intermediate fluids. For the negative spreading system, the injected fluid (gas) is the nonwetting fluid while for the positive spreading system the injected fluid is the intermediate fluid. This has important implications for the pore-scale displacement mechanisms, as will be discussed below.

III. DISPLACEMENT MECHANISMS

The three-phase displacements of interest in the present study all involve the injection of a nonwetting fluid (fluid 1 or fluid 2) into a porous medium which initially contains only wetting fluid and one other nonwetting fluid. Although regions of the pore space may be occupied by one, two, or all three fluids simultaneously, individual displacements all involve an invasion of a pore throat or pore body by a *two-phase* interface as in two-phase flow. Displacements in three-phase flow may therefore be completely described by a simple generalization of well understood two-phase displacements.

Two-phase displacements are either drainage or imbibition processes. Drainage, or the invasion of a nonwetting fluid, occurs when invading nonwetting fluid displaces defending wetting fluid from a pore throat. For a pore throat of inscribed radius r_t, this requires a threshold capillary pres-

TABLE II. Two-phase displacements in three-phase flow.

Drainage processes		Threshold capillary pressure ($P_{inv}-P_{def}$)		
Invading	Defending	$S_{23}^e=0$	$-2\sigma_{12}<S_{23}^e<0$	$S_{23}^e<-2\sigma_{12}$
Fluid 1	fluid 2	$\frac{2\sigma_{12}}{r_t}$	$\frac{2\sigma_{12}\cos\theta_{12}}{r_t}$	$\frac{2(\sigma_{13}-\sigma_{23})}{r_t}$
Fluid 1	fluid 3	$\frac{2(\sigma_{12}+\sigma_{23})}{r_t}$	$\frac{2\sigma_{13}}{r_t}$	$\frac{2\sigma_{13}}{r_t}$
Fluid 2	fluid 3	$\frac{2\sigma_{23}}{r_t}$	$\frac{2\sigma_{23}}{r_t}$	$\frac{2\sigma_{23}}{r_t}$

Imbibition processes		Piston	Snap-off	Piston	Snap-off	Piston	Snap-off
Fluid 2	fluid 1	$\frac{-2\sigma_{12}}{r_{imb}}$	$\frac{-\sigma_{12}}{r_t}$	$\frac{-2\sigma_{12}\cos\theta_{12}}{r_{imb}}$	–	$\frac{2\sigma_{23}}{r_p}-\frac{2\sigma_{13}}{r_{imb}}$	–
Fluid 3	fluid 1	$\frac{-2(\sigma_{12}+\sigma_{23})}{r_{imb}}$	$\frac{-(\sigma_{12}+\sigma_{23})}{r_t}$	$\frac{-2\sigma_{13}}{r_{imb}}$	$\frac{-\sigma_{13}}{r_t}$	$\frac{-2\sigma_{13}}{r_{imb}}$	$\frac{-\sigma_{13}}{r_t}$
Fluid 3	fluid 2	$\frac{-2\sigma_{23}}{r_{imb}}$	$\frac{-\sigma_{23}}{r_t}$	$\frac{-2\sigma_{23}}{r_{imb}}$	$\frac{-\sigma_{23}}{r_t}$	$\frac{-2\sigma_{23}}{r_{imb}}$	$\frac{-\sigma_{23}}{r_t}$

sure $(P_{inv}-P_{def})$ of approximately $2\sigma\cos\theta/r_t$, where θ is the contact angle formed at the invading/defending fluid interface.

Imbibition, or the invasion of a wetting fluid, allows two distinct types of displacements. The first is *pistonlike* displacement where invading wetting fluid displaces defending nonwetting fluid from pore throats and bodies. In pore throats the threshold capillary pressure is the same as for drainage. However, in pore bodies the process is limited by the largest radius of curvature r_{imb} of the wetting-nonwetting fluid interface in the pore body. This threshold curvature depends on the inscribed pore body radius r_p and the configuration of the nonwetting fluid in the adjacent throats [17]. The second imbibition process is *snap-off* where a film of wetting fluid in a pore throat swells until the wetting-nonwetting fluid interface becomes unstable and wetting fluid invades the throat. Snap-off can only occur when continuous films of the invading wetting fluid exist.

Three-phase flow allows all possible combinations of two-phase displacements. In all, there are six such two-phase displacements for all possible combinations of invading-defending fluid pairs and these are summarized in Table II. The threshold capillary pressures for these displacements depend on the fluid pair involved and on the fluid configuration in pore bodies and throats. Table II summarizes the threshold capillary pressures for each of the three basic configurations discussed earlier.

Table II shows that if the invading fluid is the nonwetting fluid, only drainage displacements can occur. If, on the other hand, the wetting fluid is the invading fluid, the displacement is always an imbibition process. The intermediate fluid is nonwetting with respect to the wetting fluid but wetting with respect to the nonwetting fluid. Displacements involving intermediate fluid as the invading fluid may thus be either drainage or imbibition processes. When the injected fluid is a nonwetting fluid (i.e., fluid 1 or fluid 2) experimental observations [11–13] suggest that displacements involving fluid 3 as the invading fluid are not favored and hardly ever occur. For the sake of brevity, these processes are therefore not considered.

For a displacement to proceed, it must be possible for invading fluid to flow to the invasion site and defending fluid to flow from the invasion site. Invading and defending fluids may flow to and from invasion sites by bulk and/or film flow. Injected nonwetting fluid flows from the inlet to the invasion site through a system of interconnected pores and throats filled with nonwetting fluid (bulk flow). The wetting fluid is hydraulically connected throughout and flows away from the invasion site through a system consisting of regions of interconnected pores and throats filled with wetting fluid (bulk flow) connected by wetting films (film flow). The manner in which the intermediate fluid flows depends on the spreading behavior. If $S_{23}^e=0$, the intermediate fluid flows in a manner exactly analogous to that of the wetting fluid with spreading films interconnecting regions of bulk intermediate fluid. If $S_{23}^e<0$, there are no intermediate fluid spreading films and the intermediate fluid flows in a manner similar to that of the nonwetting fluid, i.e., by bulk flow.

Invading fluid displaces defending fluid from invaded pore throats until it reaches the diverging pore space at the entrance to the adjoining pore body. The invading fluid may then remain stationary at the entrance to the pore, displace fluid from the pore, or coalesce with fluid in the pore body. What actually happens depends on the nature of the invading fluid, the fluids occupying the pore body, and the spreading behavior.

When the invading fluid and the fluid in the adjoining pore body are the same, the displacement results in coalescence and reconnection of invading fluid. When the two fluids are different, the invading fluid spontaneously displaces the fluid in the pore body if the invading fluid is the more strongly nonwetting. Nonwetting fluid therefore spontaneously displaces both wetting and intermediate fluids while intermediate fluid only displaces wetting fluid. When the

bulk fluid in the pore body is more strongly nonwetting than the invading fluid, the fluid in the pore body blocks the invading fluid. The invading fluid can only enter the pore body if the pressure in the invading fluid is increased sufficiently to overcome the threshold capillary pressure for the pore body. Of all the possible or available interfaces which could be advanced at any instant in time, the interface or interfaces which are actually advanced are those for which the capillary pressure exceeds the threshold pressure.

Because the wetting fluid is hydraulically connected throughout, drainage events involving the displacement of wetting fluid always result in flow of wetting fluid to the outlet. However, when a drainage event involves the displacement of intermediate fluid, the intermediate fluid may not be continuous to the outlet. Continuity then requires that the first displacement (nonwetting-intermediate) is associated with a second displacement in which displaced intermediate fluid displaces wetting fluid to the outlet. Øren, Billiote, and Pinczewski [11] refer to this as a *double-drainage* displacement, with the displacement sequence fluid 1→fluid 2 →fluid 3. The other displacement process which is observed in the micromodel experiments is in the case $S_{23}^{e} < -2\sigma_{12}$. In this case a thin film of fluid 3 (wetting fluid) separates the other two fluids (nonwetting fluids). Thus the drainage mechanism in this case is a forced drainage-imbibition process with the displacement sequence fluid 2→fluid 1 →fluid 3. In both of the above processes the overall capillary pressure that must be overcome for the combination of events to occur is given by the sum of the capillary pressure of the individual two-phase displacements as given in Table II. Note in the experimental micromodels no displacements are seen where the fluid invading a pore is the wetting fluid. This is because the injected phase is never a (strongly imbibing) wetting fluid. Thus this case is never considered in our numerical model.

Double displacements involving flow through spreading films may be expected to be rate sensitive and strongly dependent on fluid topology (saturation history). For high displacement rates, the pressure drops associated with film flow are large and may therefore have a significant influence on the capillary pressures at displacement sites. This is particularly true for double-drainage displacements where threshold capillary pressures for second drainage events may only be exceeded at sites in close proximity to the sites of the first drainage events, i.e., at sites associated with the invaded cluster where the intermediate fluid may flow by bulk flow. The nature of the displacement for systems with spreading films may then be expected to be similar to that for systems where there are no spreading films. For low displacement rates, film pressure drops may be sufficiently small for the displacement to be dominated by capillary pressure. The sites of the first and second drainage events are then determined primarily by the pore throat size distribution as in classical invasion percolation. Intermediate displacement rates will display behavior intermediate between these two limits.

For the experimental systems being considered, our computational observations suggest that the majority of individual displacements are drainage events. The one exception to this occurs in the oil-wet positive spreading system where the injected fluid is the intermediate fluid. In this case, frequent intermediate-nonwetting fluid piston-type displacements occur. The major difference between this displacement and the two-phase drainage mechanism which occurs in all systems is the different threshold pressure condition which must be satisfied (see Table II).

IV. NUMERICAL MODEL

The porous medium is represented by a simple two-dimensional network of sites and bonds. The sites or nodes correspond to pore bodies and represent the entire void volume of the porous medium (porosity). The bonds or links correspond to the pore throats and represent the medium resistance to flow (permeability). The bonds are considered to have negligible volume. Similar descriptions have been used to model the porous medium in previous two-phase flow studies by Lenormand, Touboul, and Zarcone [27], Blunt and King [18], Blunt, King, and Scher [19], and Jerauld and Salter [20].

In order to allow multiple fluids to occupy the pore space simultaneously, bonds are modeled as long narrow channels of lenticular cross section. The channels are of constant length l, uniform depth d, and width x_t. The width x_t for each link is chosen randomly from a specified distribution function. The nodes are also assumed to be lenticular in cross section with constant depth d and width x_b ($x_b > x_t$) which may also be randomly distributed.

The above description of the porous medium allows all the important experimentally observed features of three-phase flow to be modeled. These include the random distribution of link threshold pressures, the existence of wetting and spreading films, and the dependence of film thickness on the prevailing capillary pressure.

Flow in the network is modeled on the basis of the pore-scale physics described above. This physics is implemented by making the usual assumptions that have been used for modeling two-phase flow, but generalizing them in an obvious manner for our purposes. First we assume the fluids are Newtonian, incompressible, immiscible, and the flow is everywhere laminar (Poiseuille flow). All the fluid volumes are allocated to the nodes and all the pressure drops are allocated to the links connecting the nodes. In contrast to two-phase flow, where only two fluids may be present in links and nodes, we allow links and nodes to be occupied by all three fluids simultaneously. However, only one of the fluids, the bulk fluid, can be displaced. The other fluids are present as wetting and/or spreading films. Volume changes of films in nodes are considered to be negligibly small.

The nodes are divided into two groups—*full nodes* and *interface nodes*. Full nodes are nodes which are not being invaded and are occupied by a single bulk fluid with the other fluids present as wetting and/or spreading films. On the other hand, interface nodes are nodes which are being invaded and may be occupied by two or three bulk fluids simultaneously. The contents of an interface node change with time. The fluid pressures are only calculated in nodes and the nodes are considered to be sufficiently large for the capillary pressure across the invading interface(s) in the node to be zero. That is, the invading and defending fluid pressures in a node are the same.

To determine the fluid phase pressures we must define the

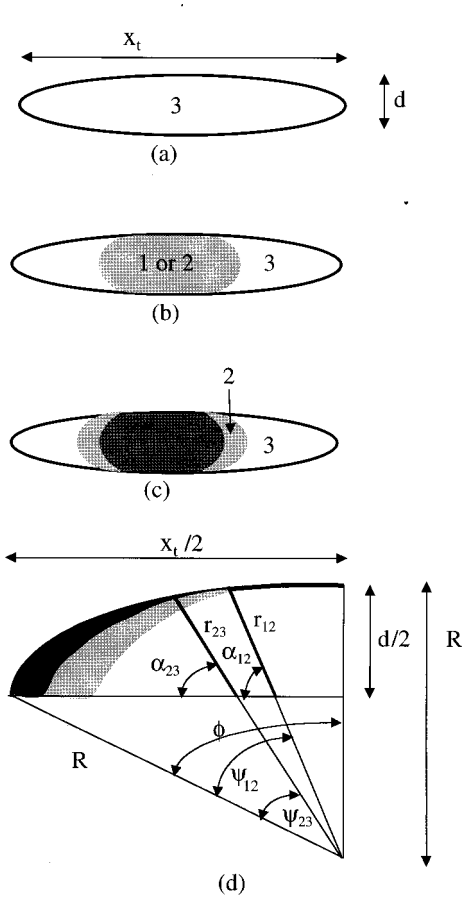

FIG. 2. Schematic of fluid distributions in an eye-shaped link occupied by (a) one, (b) two, (c) three fluids. In (d) we show the construction of the intermediate spreading and wetting films in the link. The lenticular throat has constant length l in the direction perpendicular to the page.

continuity of each phase in the network. If a fluid is present as bulk or film in two or more links connected to a node then it is considered continuous across the node if the following are true.

(1) It is the wetting fluid.
(2) It is the intermediate fluid and $S_{23}^{e}=0$.
(3) The node is occupied by the same fluid.

Although the volumes of fluids in links are assumed to be negligible, the distribution of these fluids in links is important in determining the resistances to flow through the network. Links may be occupied by one, two, or all three fluids simultaneously. However, capillary pressure dictates that the bulk of a link is only occupied by a single fluid. We refer to the link as being occupied by this fluid. The other fluids may be present as wetting and/or spreading films.

A schematic representation of the three possible fluid distributions over the cross section of a link is shown Fig. 2. In Fig. 2(a) the link is occupied only by wetting fluid. In Fig. 2(b) the link is occupied by one of the nonwetting fluids (fluid 1 or fluid 2) with wetting fluid present as a wetting film. Figure 2(c) shows a link occupied by the nonwetting fluid with wetting and intermediate fluids present as wetting and spreading films, respectively. The latter configuration is only possible when $S_{23}^{e}=0$ (i.e., in the water-wet, positive spreading system).

Figure 2 illustrates the important role played by the fluid distribution in links in controlling the flow of fluids in three-phase flow. Although as many as all three fluids may be flowing simultaneously through a link, capillary pressure determines that only one of the fluids is transported by bulk flow. The other fluids must flow through films.

The simultaneous flow of one, two, or three fluids through a link is complicated by the geometry of the cross-sectional area open to flow and the fact that the flows of individual fluids are coupled by momentum transfer across the fluid-fluid interfaces. A further complication is that the flows may not be unidirectional. Although the coupled flow problem is not difficult to model, the solution can only be obtained by numerical means at considerable computational expense. In the present treatment we make the simplification that the resistance to the flow of fluid i in a link may be characterized by the concept of a mean hydraulic radius $\mathcal{R}_i$, given by

$$\mathcal{R}_i=\frac{2\mathcal{A}_i}{\mathcal{P}_i}, \tag{6}$$

where $\mathcal{A}_i$ is the cross-sectional area for flow and $\mathcal{P}_i$ is the wetted perimeter for fluid i in the link.

Thus to calculate the hydraulic radius we need both $\mathcal{A}_i$ and $\mathcal{P}_i$. To obtain these consider Fig. 2(d), which is drawn for the most complicated case, where three fluids are simultaneously present in a link. The cross-sectional area open to flow for each of the fluids present can be determined from elementary geometry to be

$$\mathcal{A}_3=2\psi_{23}R^2-2R(R-r_{23})\sin\psi_{23}-2\alpha_{23}r_{23}^2 \tag{7}$$

for the wetting film,

$$\mathcal{A}_2=2(\psi_{12}-\psi_{23})R^2-2R(R-r_{12})\sin\psi_{12}-2\alpha_{12}r_{12}^2 +2R(R-r_{23})\sin\psi_{23}+2\alpha_{23}r_{23}^2 \tag{8}$$

for the intermediate spreading film, and

$$\mathcal{A}_1=2\phi R^2-\left(R-\frac{d}{2}\right)x_t-2\psi_{12}R^2+2R(R-r_{12})\sin\psi_{12} +2\alpha_{12}r_{12}^2 \tag{9}$$

for the bulk nonwetting fluid. In the above equations,

$$R=(x_t^2+d^2)/4d,$$

$$\sin\phi=x_t/2R,$$

$$\sin\alpha_{12}=(R-d/2)/(R-r_{12}),$$

$$\sin\alpha_{23}=(R-d/2)/(R-r_{23}),$$

$$\psi_{12}=\phi+\alpha_{12}-\pi/2,$$

$$\psi_{23}=\phi+\alpha_{23}-\pi/2.$$

The wetted perimeter (fluid-fluid and solid-fluid interfaces) for each fluid is also readily determined from elementary geometry. For the wetting film we obtain

$$\mathcal{P}_3 = 4\psi_{23}R. \tag{10}$$

In the case of a positive spreading system with the link occupied by all three fluids, the wetted perimeter for the intermediate fluid spreading film is

$$\mathcal{P}_2 = 4(\psi_{12} - \psi_{23})R. \tag{11}$$

The above equation is based on the assumption of negligible viscous losses at the fluid-fluid interfaces. Finally, for the bulk nonwetting fluid we obtain

$$\mathcal{P}_1 = 4\left(\frac{\pi}{2} - \alpha_{12}\right)R + 4\alpha_{12}r_{12}, \tag{12}$$

where all the boundaries (fluid-fluid and fluid-solid) are considered to contribute to the viscous losses. Similar equations may be written for the other systems where the link may be occupied by two fluids. For a link occupied only by wetting fluid, the wetted perimeter is simply,

$$\mathcal{P}_3 = 4\phi R. \tag{13}$$

In the above equations we require the radius of curvature of the wetting film interface, r_{23}, and that of the spreading film interface, r_{12}. These are given by the Young-Laplace equation,

$$r_{12} = \frac{\sigma_{12}}{P_1 - P_2}, \tag{14}$$

$$r_{23} = \frac{\sigma_{23}}{P_2 - P_3}, \tag{15}$$

where P_1, P_2, and P_3 are the pressures of fluids 1, 2, and 3 in the link. Since fluid pressures are only defined at nodes, these are interpolated from the neighboring node pressures.

When the injected fluid is a nonwetting fluid (fluid 1 or fluid 2), experimental observations suggest that fluid 3 is always a defending fluid. Invasion of links and nodes by fluid 3 is therefore not considered. The conditions which must be satisfied for a link *IJ*, containing defending fluid *j*, to be invaded by fluid *i* follow.

(1) The pressure difference between invading fluid *i* in node *I* and defending fluid *j* in node *J* must exceed the link threshold capillary pressure,

$$P_{i,I} - P_{j,J} > P_{c,ij,IJ}, \tag{16}$$

where $P_{c,ij,IJ}$ is the threshold capillary pressure for the invading interface in link *IJ* which is given for the various configurations in Table II.

(2) The defending fluid in the link must be able to leave the link by either bulk or film flow. If defending fluid cannot leave the link, the fluid is trapped. Trapping only occurs in systems where $S_{23}^e < 0$. Defending fluid 1 or fluid 2 may then be trapped in a link connecting two nodes occupied by the injected fluid.

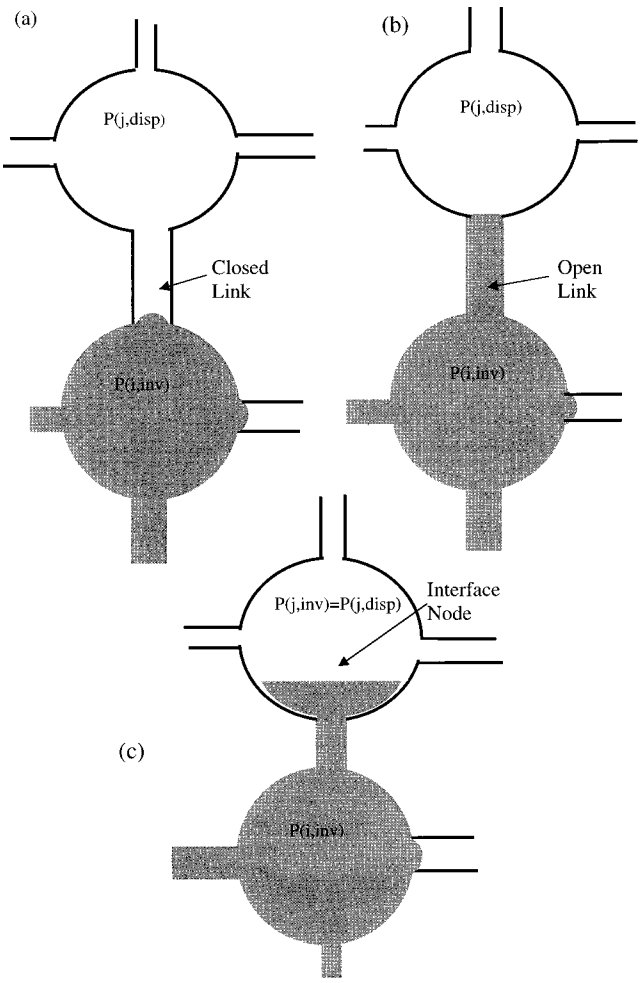

FIG. 3. Possible configurations of the interface between the invading and displaced fluids. (a) The capillary threshold pressure has not been exceeded and the link is closed, i.e., $P(i,\text{inv}) - P(j,\text{disp}) < P(\text{entry},ij)$. (b) The capillary pressure is exceeded and the link is opened, i.e., $P(i,\text{inv}) - P(j,\text{disp}) > P(\text{entry},ij)$. (c) The adjacent node becomes an *interface* node.

When the above two conditions are satisfied, the link is said to be *open* to the invading fluid and the invading fluid immediately enters the link. Otherwise, the link is *closed* and the interface remains stationary at the entrance to the link (see Fig. 3).

The specific consequences of a link opening depend on the nature of the invading fluid, the fluid occupying the adjacent node, and the spreading behavior. When the invading fluid and the fluid occupying the node are the same, coalescence occurs and the displacement is considered to be complete. If the two fluids are different, the invading fluid can only enter the node if the pressure difference between the invading fluid *i* in link *IJ* and the defending fluid *j* in node *J* exceeds the node threshold capillary pressure,

$$P_{i,I} - P_{j,J} > P_{c,ij,J}. \tag{17}$$

When the above condition is satisfied, the invading fluid immediately enters the node, which then becomes an *interface*

node. We note that for drainage events, the threshold pressure for a node is always less than that for a connecting link. Invading nonwetting fluid thus spontaneously invades both wetting and intermediate fluid occupied nodes while intermediate fluid only spontaneously invades nodes occupied by the wetting fluid. For piston-type imbibition events, the node threshold pressure is always larger than that for a connecting link. Consequently, invading intermediate fluid only invades nonwetting fluid occupied nodes if the pressure in the intermediate fluid is increased sufficiently to overcome the node threshold pressure. The node threshold pressures for the different fluid configurations are given in Table II.

To calculate the individual nodal pressures the displacements are treated using the usual quasi-static approximation. That is, the fluids flow through the network at a constant rate in response to computed pressure distributions in each of the three fluids over a time step Δt. The time-step size is selected so that only one interface node is completely displaced at the end of each time step. Since a number of interface nodes may be undergoing invasion simultaneously, we identify all the interface nodes $\{I\}$ which are filling and determine the time required for each node to be completely displaced using flow rates from the computed pressure distribution. The minimum displacement time corresponds to Δt, i.e.,

$$\Delta t = [\Delta V_I^D / Q_I]_{\min}, \tag{18}$$

where ΔV_I^D is the volume of defending fluid in node I at the beginning of the time step and Q_I is the total displacement rate.

The flow through link IJ is related to the pressures in the neighboring nodes ($P_{i,I}$ and $P_{i,J}$) by

$$Q_{i,IJ} = g_{i,IJ}(P_{i,I} - P_{i,J}), \tag{19}$$

where $g_{i,IJ}$ is the conductivity of fluid i in a link IJ, which is given by

$$g_{i,IJ} = \frac{\pi \mathcal{R}_{i,IJ}^4}{8 \mu_i l}. \tag{20}$$

Since the fluids are incompressible, continuity requires that at each node

$$\sum_J Q_{i,IJ} = 0, \tag{21}$$

where J runs over all links connected to node I. Equations (19)–(21), together with the appropriate initial and boundary conditions, form a complete solution to the flow of fluids in the network. The nodal pressures for each fluid are determined by *successive over relaxation* (SOR) using a routine written by Colgan [28],

$$P_{i,I} = \omega \frac{\Sigma_J g_{i,IJ} P_{i,J}}{\Sigma_J g_{i,IJ}} + (1-\omega) P_{i,I}, \tag{22}$$

where, again, the sum over J refers to all the links connected to node I and ω is the over-relaxation parameter.

We now define our initial and boundary conditions. For the displacements of interest in the present study, the network initially contains only wetting fluid and one of the nonwetting fluids. The initial fluid distribution arises as a result of a two-phase imbibition displacement, for the water-wet systems, and a two-phase drainage displacement for the oil-wet systems, which precede the gas flood. Fluid is injected at a constant rate $Q_{1,\mathrm{inj}} = \Sigma_J Q_{1,0J}$, where the subscript 0 identifies the injected fluid reservoir which is attached by links $0J$ to nodes J along the inlet to the network. The wetting fluid pressure at the outlet nodes, $P_{3,NJ}$, is arbitrarily set to zero. The edges of the network are impermeable boundaries and flows in links connected to these boundaries are set to zero.

The displacement is driven by increasing capillary pressure. Capillary pressure increases as a consequence of the injection of nonwetting or intermediate fluid. In the computations, the injected fluid pressure is increased at the beginning of each new time step by a small increment so that at least one new node is invaded over the time step. In order to solve for the individual fluid pressures using Eq. (22), we must first identify the boundaries or the extent of each of the three fluids in the network.

Wetting fluid. Since the wetting fluid is continuous throughout the network, Eq. (22) is applied at all nodes other than those at the outlet where the pressure is arbitrarily set to zero.

Injected fluid. The injected fluid is either intermediate fluid (oil-wet, positive system) or nonwetting fluid (other systems). Like the wetting fluid, the injected fluid is also continuous. However, it only occupies part of the network at any instant in time. At the start of the displacement, the injected fluid is present only at the inlet nodes. As the displacement progresses, it progressively occupies an increasing number of nodes in the network. Again, Eq. (22) is used to update the nonwetting fluid pressures in these nodes.

Second nonwetting fluid. The second nonwetting fluid is either the nonwetting fluid (oil-wet, positive system) or the intermediate fluid (other systems). Unlike the other two fluids, the second nonwetting fluid may initially exist as a number of disconnected or isolated clusters. These clusters are immobile because the capillary number (ratio of viscous to capillary forces) for the displacement is low. Pressures for this fluid are only calculated for clusters being invaded. For systems with $S_{23}^e < 0$, these are clusters of fluid which share an interface with the injected fluid. For systems with $S_{23}^e = 0$, where the injected nonwetting fluid is contained entirely within the intermediate fluid, it is only necessary to identify a single cluster which consists of all the interconnected nodes and links occupied by intermediate and nonwetting fluids. During the course of the displacement, isolated clusters of intermediate fluid may become reconnected by coalescence. It is therefore necessary to update the extent of the clusters at the commencement of each pressure solution.

Three-phase algorithm

Finally we briefly detail the sequence of our three-phase algorithm, based on the preceding discussion. The solution for the three fluid pressures is iterative because the individual fluid pressures are coupled through the pressures in interface nodes where the bulk fluid pressures are equal, and because

it is necessary to specify *a priori* which links are open and which are closed to invading fluids. The procedure for each time step Δt is as follows.

(i) The pressure for each fluid in every node containing the fluid is calculated using Eq. (22).

(ii) The computed pressures are used to calculate capillary pressures for each closed link, using Eq. (16) or Eq. (17). Links for which the capillary pressure exceeds the threshold pressure are opened and the pressure solution is recalculated to check that these links remain open.

(iii) The pressures are then used to calculate link flow rates for all links attached to interface nodes using Eq. (19). Links which have a negative flow rate are deleted from the set of open links and the pressure solution is recalculated. This procedure is iterated until the capillary pressures are consistent with the flow rates in the network.

(iv) The link flow rates are used to determine the time-step size Δt, using Eq. (18), and to update interface node fluid volumes or saturations using

$$V_i|_{t+\Delta t} = V_i|_t + \Delta T \sum_J Q_{i,IJ}, \tag{23}$$

where V_i is the volume of invading fluid in node I.

(v) The injected fluid pressure is incremented and the above procedure is repeated for the next time step.

This algorithm has not been optimized for computational efficiency. For example, to simulate one gas flood took roughly three to four days on a Silicon Graphics Indigo Machine. Up to 95% of the computation is spent in the pressure solver and to get convergence of the order of 10 000 iterations are required. Clearly to proceed to larger grids and higher dimensions significant effort has to be expended to improve the algorithm's efficiency.

V. SIMULATION RESULTS AND DISCUSSION

The network simulator was validated by comparing simulated fluid recoveries with those measured in the glass micromodel displacement experiments reported by Øren, Billiote, and Pinczewski [11] (water-wet systems) and Øren and Pinczewski [13] (oil-wet systems). These experiments consisted of a number of quasistatic tertiary immiscible gas floods (three-phase displacements) to recover water-flood residual oil under both oil-wet and water-wet conditions. A complete description of the experiments, the glass micromodel, and the fluids used is given by Øren and co-workers [11–13]. In what follows we use this information to specify the fluid and network parameters for the simulations.

The parameters used for our numerical simulations mimicked the experimental situation. The viscosities of the oil and water were 1.4 and 1.0 cP, respectively. The viscosity of the gas (air) was much lower and for the purpose of the simulations the gas is considered to be inviscid. The interfacial tensions for the positive and negative spreading systems are given in Table I. The three-phase contact angle for the water-wet, negative spreading system is estimated to be $\theta_{12} = 52°$, while for the oil-wet, negative spreading system it is estimated to be $\theta_{12} = 89°$.

The glass micromodel used in the experiments consisted of approximately 4600 intersecting capillaries on a 50×50 square grid at 45° to the flow direction from the inlet to the outlet. The capillaries were approximately eye shaped in cross section, having a depth d of approximately 150 μm. For the purpose of the simulations, the depth is considered to be constant. The length of the throats or links was assumed to be constant with $l = 500\ \mu$m. There was a slight difference in pore/throat sizes between water-wet and oil-wet displacements. For the water-wet displacements the width of the pore bodies or nodes was chosen randomly from a uniform distribution ($x_b \in [300\ \mu\text{m}, 400\ \mu\text{m}]$). The width of the links was randomly selected from a uniform distribution ($x_t \in [100\ \mu\text{m}, 140\ \mu\text{m}]$). For the oil-wet displacements the width of the nodes was chosen randomly from a uniform distribution ($x_b \in [350\ \mu\text{m}, 450\ \mu\text{m}]$), while the width of the links was randomly selected from a uniform distribution ($x_t \in [160\ \mu\text{m}, 240\ \mu\text{m}]$). In addition, for the oil-wet displacements, throat widths in the capillary barrier at the outlet were made very narrow ($\approx 100\ \mu$m) to prevent early breakthrough in the initial water-flood drainage. The effect of different pore geometries, i.e., sharper or rounder corners, has not been investigated in detail here, but one would expect that these effects could significantly alter recoveries.

The initial distribution of oil and water was established by simulating a low rate two-phase imbibition displacement for the water-wet systems and a low rate two-phase drainage displacement for the oil-wet systems. This was done using two-phase versions of the three-phase model which included flow through wetting films. Since the gas is considered to be inviscid, the pressure in the gas is everywhere constant and the procedure outlined in the preceding section for calculating fluid pressures is somewhat simplified since it is only necessary to solve for two of the three fluid pressures.

We first compare our numerical simulation results with the experimental displacements. The computed and experimentally determined oil and water recoveries for the tertiary gas displacements are compared in Table III for both the water-wet and oil-wet systems. Considering the necessarily approximate nature of the estimates for the model input parameters and the necessity to establish the initial conditions by a two-phase network simulation, the agreement between the experiments and the computations is encouraging. Although the computed recoveries are the average of only ten realizations, the comparison clearly shows that the three-phase network simulator faithfully reproduces all the experimentally observed characteristics of the three-phase displacements and correctly predicts the important role of film flow on the recovery of water-flood residual oil.

Table III shows that the highest oil recoveries are obtained for the oil-wet systems (approximately 85%). The uniformly high oil recoveries are the result of flow through continuous oil-wetting films which are present throughout the entire porous medium in both the positive and negative systems. This result is different to that for the water-wet systems where the absence of oil spreading films for the negative system results in a significantly lower oil recovery (approximately 14%) than for the corresponding positive system (approximately 40%). The large difference in oil recovery for

TABLE III. Comparison between computed and experimental three-phase displacements. Computed results are averaged over ten independent realizations. The errors are ±1 standard deviation. Note experimental results are for only one flood each, but Øren and co-workers [11,13] believe these are quite reproducible.

Water-wet, negative spreading system	Computed	Experimental
Water-flood residual oil saturation as a percentage of lattice volume	60±6	62
Oil recovered by tertiary gas flood as a percentage of initial residual	14±7	18
Water recovered by tertiary gas flood as a percentage of initial residual	68±12	72
Water-wet, positive spreading system	**Computed**	**Experimental**
Water-flood residual saturation as a percentage of lattice volume	60±6	62
Oil recovered by tertiary gas flood as a percentage of initial residual	41±12	40
Water recovered by tertiary gas flood as a percentage of initial residual	61±12	69
Oil-wet, positive spreading system	**Computed**	**Experimental**
Water-flood residual saturation as a percentage of lattice volume	40±2	42
Oil recovered by tertiary gas flood as a percentage of initial residual	85±1	74
Water recovered by tertiary gas flood as a percentage of initial residual	62±4	60
Oil-wet, negative spreading system	**Computed**	**Experimental**
Water-flood residual oil saturation as a percentage of lattice volume	40±2	41
Oil recovered by tertiary gas flood as a percentage of initial residual	84±2	84
Water recovered by tertiary gas flood as a percentage of initial residual	61±4	62

the positive and negative systems under water-wet conditions is primarily due to the role played by intermediate-fluid spreading films in reconnecting the intermediate fluid for positive systems. Water-wetting films play a similar role to oil-wetting films and water recoveries for the water-wet displacements are uniformly high and of similar magnitude to the oil recoveries for the oil-wet systems.

The important role played by topological effects in determining intermediate fluid recovery is illustrated by comparing the tertiary recoveries for the intermediate fluid given in Table III. Topological effects depend on phase saturations and determine the bulk connectivity and the ease with which the intermediate fluid may be reconnected. For the oil-wet, negative system the intermediate-fluid (water) saturation is high (60%) and water is initially present as one dense cluster which spans the entire network. Displacement and reconnection of intermediate fluid is then relatively easy and its recovery is high (61%). In contrast, for the water-wet, negative system the intermediate fluid (oil) saturation is low and oil is present as disconnected clusters. Intermediate fluid is therefore difficult to reconnect and its recovery is low (14%).

The computations confirm the experimental observations that high oil recoveries in tertiary gas displacements are associated with the presence of oil films (wetting or spreading films). Although the computed conductivities for both the wetting and spreading films are only of the order of 1% of the corresponding values for a fully saturated link, fluid flow through these films is clearly important in determining fluid recovery in the micromodel displacements.

Overall behavior. Water-wet systems. Figure 4 shows the computed progress of a tertiary gas flood for the case of a negative spreading system while Fig. 5 shows the corresponding case for the positive spreading system. The initial oil saturation was 63% for both simulations. Although the initial conditions were identical, the progress of the three-phase displacements and the fluid recoveries for the two cases are clearly different.

For the negative spreading system, there is initially little difference in the preference between gas-oil-water (double drainage) and gas-water (direct two-phase displacement) displacements. As a result, the injected gas readily bypasses water-flood residual oil. Water in the neighborhood of the bypassed oil becomes more difficult to displace because previously water filled pores are now occupied by gas, which blocks high conductivity water paths. The loss of high conductivity water paths increases the water pressure and makes

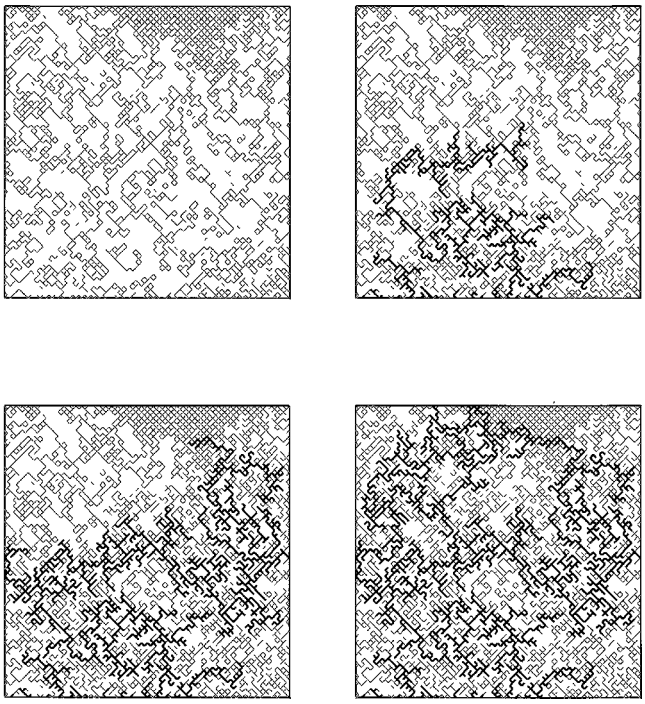

FIG. 4. Computed progress of a three-phase displacement for the water-wet negative spreading system (initial oil 63%, oil recovery 19%, water recovery 80%; gas in thick lines, oil in thinner lines, and water in white). In this figure, and the following three, the progress of the gas flood is from left to right and top to bottom.

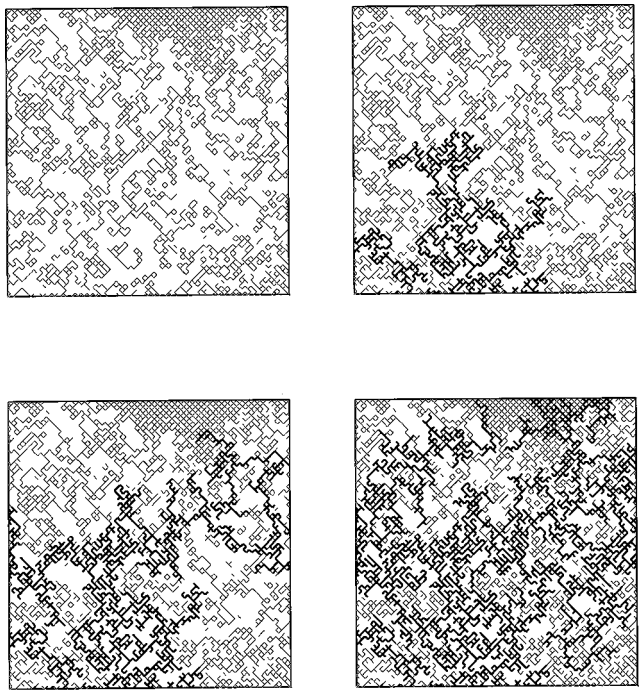

FIG. 5. Computed progress of a three-phase displacement for the water-wet positive spreading system (initial oil 63%, oil recovery 46%, water recovery 72%; gas in thick lines, oil in thinner lines, and water in white).

it more difficult for gas to displace the bypassed oil by a double drainage displacement. This, in turn, makes direct gas-water displacements ahead of the isolated oil the preferred displacement mechanism. The overall effects are a low oil recovery (19%) and a high water recovery (80%).

For the positive spreading system, oil spreading films reconnect all the oil contacted by gas. This greatly increases oil connectivity as well as the number of accessible oil-water interfaces for the second drainage event. This increased accessibility tends to make double-drainage displacements the preferred displacement mechanism. Furthermore, displaced oil at the head of the gas front may flow through spreading films to advance an oil-water interface behind the front. Oil initially bypassed by the gas may thus be reconnected and potentially recovered at a later stage in the flood. As a result, oil recovery increases to 46% compared to only 19% for the negative spreading system where the absence of oil films leaves bypassed oil disconnected and therefore trapped.

Oil-wet systems. The simulation results for the oil-wet positive and negative spreading systems were similar. In both systems the preferred displacement is a direct gas-oil displacement, since this event has the lowest threshold capillary pressure. However, because the oil saturation is low (40%) and the fact that the oil is present as a few isolated clusters surrounded by water, the most frequent displacement is a gas-water-oil double displacement.

Figure 6 shows the computed progress of the tertiary gas flood for the oil-wet, positive spreading system. The progress for the negative spreading system was similar. Initially gas contacts water and begins to invade the water cluster, resulting in water recovery at the outlet. The advance of the invading gas front is quite uniform, with no dominant fingers developing. This is due to two factors. First, since the water cluster is dense and continuous, there are many paths for water to escape to the outlet and water is rarely trapped. Secondly, the presence of isolated oil clusters serves as a barrier to gas fingers forming. As soon as gas contacts oil it tends to invade the oil cluster completely before reinvading water. This can be seen clearly in Fig. 6. As a result, both water and oil recoveries are high at 62% and 83%, respectively.

Finally, we consider how fluid recoveries depend on the initial conditions (i.e., the conditions after the water flood). For the water-wet systems we reduced the initial water-flood oil saturation to 50% (compared with 60% from before). Although the water recoveries remained largely unchanged ($\approx$70%), the reduction in initial oil saturation results in a reduction in oil recovery from 19% to 2% for the negative spreading system and from 46% to 28% for the positive spreading system. Again, flow through oil films allows a relatively high oil recovery for the positive spreading compared to that for the negative spreading system.

In the oil-wet system we increased the initial water-flood oil saturation to 65%. To achieve this we increased the width of the throats in the capillary barrier, thus permitting much earlier breakthrough than before. The water structure that results (see Fig. 7) is much less dense and very few water paths exist which completely span the lattice. Therefore, we now observe severe fingering of gas through water, leading to a lot of trapping of the water. As before, when gas meets an oil cluster, it completely invades the cluster before proceeding to invade water. The overall effect of this is a much lower water recovery (12%), compared to approximately 60% from before, but a similar oil recovery (86%).

The saturation trajectories for the displacements shown in

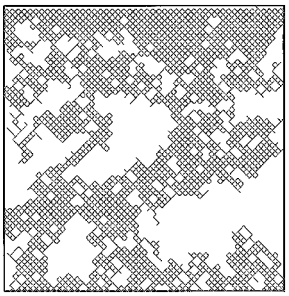

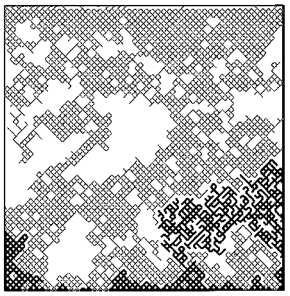

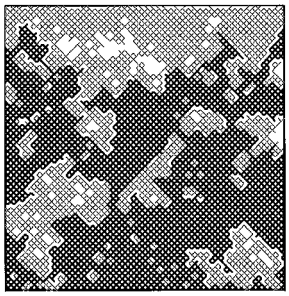

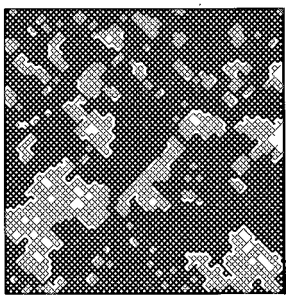

FIG. 6. Computed progress of a three-phase displacement for the oil-wet positive spreading system (initial oil 40%, oil recovery 83%, water recovery 62%; gas in thick lines, water in thinner lines, and oil in white).

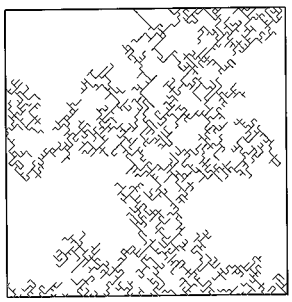

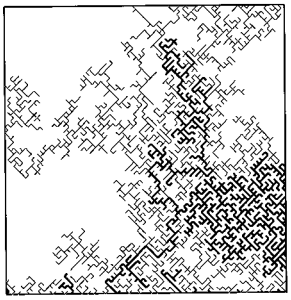

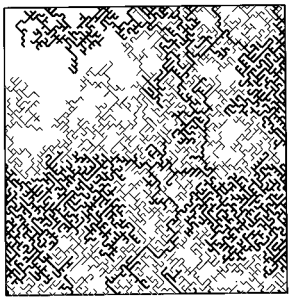

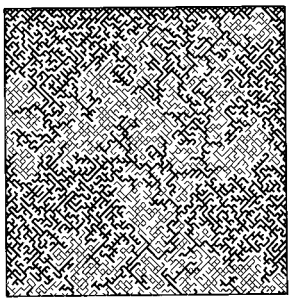

FIG. 7. Same as in Fig. 6 except for oil-wet negative system and different initial conditions (initial oil 65%, oil recovery 85%, water recovery 12%; gas in thick lines, water in thinner lines, and oil in white).

Figs. 4–7 are plotted in Fig. 8. From these saturation trajectories it is clear the wetting fluid is always preferably displaced, i.e., trajectories run roughly parallel to the wetting fluid axis, for the majority of the displacement. This is especially true for the trajectory corresponding to Fig. 7. In this case almost all the displacement events are direct gas-oil displacements. In comparison the trajectory for Fig. 7 shows significant water recovery at the end of the displacement. This is due to the dense, well connected water structure that results from the initial water flood.

In Figs. 9(a)–9(d) we plot the scaled capillary pressure as a function of gas saturation, for the systems shown in Figs. 4–7. The scaled capillary pressure P is defined as $P \equiv P_{\mathrm{cap}}/P_{\mathrm{cap}}^{\mathrm{direct}}$. Here P_{cap} is the capillary pressure for any event, and $P_{\mathrm{cap}}^{\mathrm{direct}}$ is the (arithmetic) average direct displacement (gas-wetting fluid) capillary pressure. The curves are averages over the ten realizations. In Figs. 9(a), 9(c), and 9(d) we plot two capillary pressure curves, one for the direct

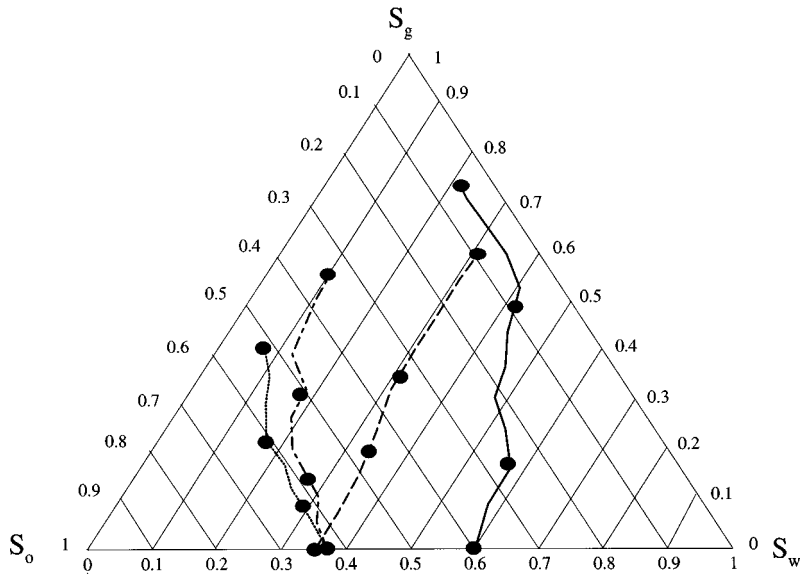

FIG. 8. Ternary diagram plotting saturation trajectories for the floods shown in Figs. 4–7. Dotted line corresponds to Fig. 4, dot-dashed line corresponds to Fig. 5, full line corresponds to Fig. 6, and dashed line corresponds to Fig. 7. Filled in circles are saturations corresponding to snapshots in Figs. 4–7.

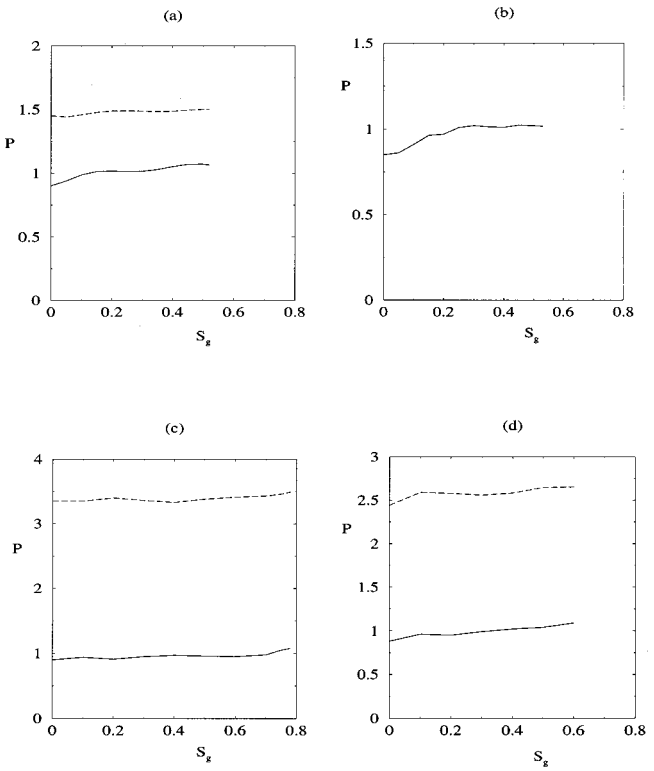

FIG. 9. Scaled capillary pressure, $P \equiv P_{\mathrm{cap}} / P_{\mathrm{cap}}^{\mathrm{direct}}$ versus gas saturation. Curves are averages over ten realizations. (a) Water-wet negative system, (b) water-wet positive system, (c) oil-wet positive system, (b) oil-wet negative system, but with initial oil saturation of approximately 60%. Full line is for direct displacement capillary pressure and dashed line is for double displacement capillary pressure. See text for further explanations.

displacement events and the second for the double displacement events. In Fig. 9(b) all displacements (either direct or double displacement) are gas-oil-water displacements. As such the interfacial tensions for these events are the same, i.e., $\sigma_{go} + \sigma_{ow}$, and so only one curve is plotted. The curves show a gradual increase, on increasing gas saturation. Finally in Fig. 10 we plot, for comparison, the capillary pressure curve corresponding to the flood shown in Fig. 6. The top set of points is the double-drainage capillary pressures, while the bottom set of points is direct displacement capillary pressures. There are some interesting observations to be made. The points do not occur uniformly with saturation but rather in clumps. This corresponds to our observation that gas seeks out oil clusters (low capillary pressure), and completely invades that cluster before it is forced to invade water (high capillary pressure). As well in each oil group there is a general increase in capillary pressure, as gas saturation increases. This corresponds again to gas seeking out the largest throats first. At the end of the flood we see the capillary pressure is large, corresponding to gas-oil-water displacements. This is in agreement with our saturation trajectory, which showed a large increase in water saturation at the end of the displacement.

The above results imply that recovery of the wetting fluid is independent of the initial conditions (saturation history), whereas the recovery of the intermediate fluid is strongly dependent on the initial conditions. These observations are in agreement with the conclusions of Dria, Pope, and Sepehrhoori [29] and Oak [7,8], who found, on the basis of relative permeability measurements for three-phase displacements in actual reservoir rocks, that the relative permeability of the intermediate fluid is strongly dependent on the intermediate fluid saturation at the commencement of the tertiary gas flood. The relative permeabilities of the other two phases were largely insensitive to saturation history.

VI. CONCLUSIONS

In this study we have put in place a numerical simulation model to describe three-phase drainage dominated fluid flow in strongly wet porous media. The model is based on the pore-scale mechanisms detailed by Øren and co-workers [11–13]. However, the double-drainage mechanism previ-

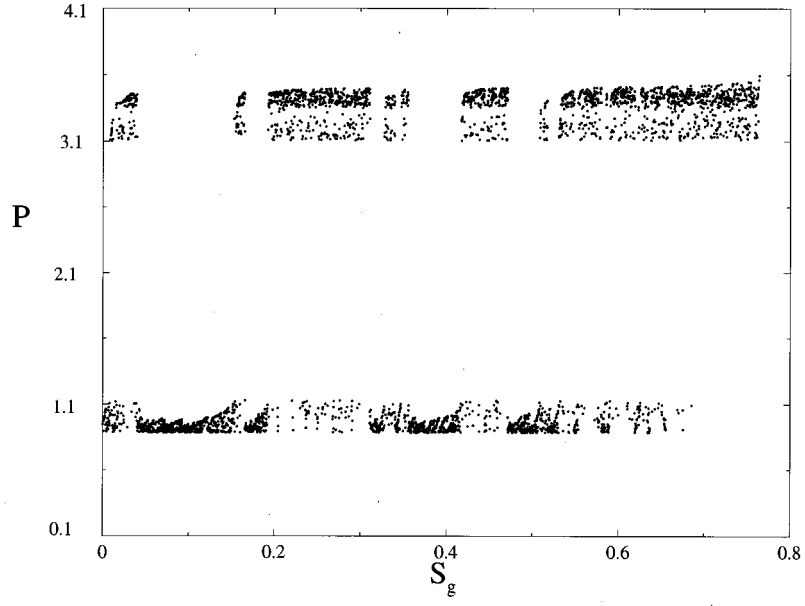

FIG. 10. Scaled capillary pressure versus gas saturation for flood shown in Fig. 6. Upper set of points corresponds to double-drainage displacements while lower set of points corresponds to direct drainage displacements.

ously used by these authors to describe three-phase displacements may be simply viewed as a two-phase displacement in which the defending fluid is not continuous to the outlet. Continuity then requires that such displacements are associated with a second drainage event(s) in which the defending fluid for the first drainage event becomes the invading fluid for the second drainage events.

As for two-phase fluid flow, flow through wetting films in corners or surface roughness is an important characteristic in determining fluid recoveries. Furthermore, correctly taking into account the high viscous pressure drops that occur in these films leads to multiple filling and emptying of pores. In our numerical model these pressure drops are calculated by solving the fluid flow equations, so that no *ad hoc* rules need be introduced as in previous studies, e.g., Øren and Pinczewski [14]. In contrast Øren and Pinczewski [14] accounted for pressure drops by ''counting'' path lengths to the outlet and then multiplying by arbitrary factors, which had no physical basis, to account for film flow or bulk flow. As such the algorithm presented here should be able to more accurately predict experimental data because all pressure drops are accounted for accurately.

The results from our numerical model closely match the experimental results of Øren and Pinczewski. Furthermore, the model shows that the displacement behavior of the intermediate fluid is strongly dependent on the saturation history of the displacement. This observation is in qualitative agreement with previous three-phase relative permeability measurements in actual porous media. It is clear, however, that the effect of dimensionality will be quite pronounced. For example, trapping of nonwetting fluid clusters occurs quite commonly in two dimensions (2D) while in 3D this is much rarer. This clearly will have quite significant effects on the relative permeability curves. In future work we hope to extend our model to three dimensions so that realistic relative permeability and capillary pressure curves may be determined and compared with actual reservoir rocks. Finally we note that we have considered only spatially uniform wettability conditions, i.e., water wet or oil wet throughout the network. Indeed many physical systems may have mixed wettability conditions, i.e., local wettability correlated with fluid type. This situation, although more difficult to model, is clearly important and is another area for future study.

ACKNOWLEDGMENTS

The author would like to thank W. V. Pinczewski and P. E. Øren for many useful discussions and helpful comments on the manuscript. J. R. May is thanked for technical assistance. The Australian Commonwealth Government is acknowledged for their support of this work through the Cooperative Research Centres Program.

[1] M. Honarpour, L. Koederitz, and A. H. Harvey, *Relative Permeability of Petroleum Reservoirs* (CRC Press, Boca Raton, FL, 1986).
[2] H. L. Stone, J. Pet. Technol. **22**, 214 (1970).
[3] H. L. Stone, J. Can. Pet. Technol. **12**, 53 (1973).
[4] F. J. Fayers and J. D. Matthews, Soc. Pet. Eng. J. **4**, 224 (1984).
[5] J. C. Parker and R. J. Lenhard, Water Resour. Res. **24**, 2187 (1987).
[6] M. A. Aleman and J. C. Slattery, Transp. Porous Media **3**, 111 (1988).
[7] M. J. Oak, in *Proceedings of the 7th SPE/DOE Symposium on Enhanced Oil Recovery, Tulsa* (SPE, Richardson, 1990).
[8] M. J. Oak, in *Proceedings of the 66th Annual Technical Conference of the SPE, Dallas* (SPE, Richardson, 1991).
[9] B. F. Marek, K. J. Hartman, and A. E. McDonald, in *Proceedings of the SPE/DOE Middle East Oil Show, Bahrain* (SPE, Richardson, 1991).
[10] A. Kantzas, I. Chatzis, and F. A. L. Dullien, in *Proceedings of the 5th SPE/DOE Symposium on Enhanced Oil Recovery, Tulsa* (SPE, Richardson, 1988).
[11] P. E. Øren, J. Billiote, and W. V. Pinczewski, SPE Form. Eval. **7**, 70 (1992).
[12] P. E. Øren and W. V. Pinczewski (unpublished).
[13] P. E. Øren and W. V. Pinczewski, SPE Form. Eval. **9**, 149 (1994).
[14] P. E. Øren and W. V. Pinczewski, Transp. Porous Media **20**, 105 (1995).
[15] F. J-M. Kalaydjian, J-C. Moulu, O. Vizika, and P. K. Munkerud, in *Proceedings of the 68th Annual Technical Conference of the SPE, Houston* (SPE, Richardson, 1993).
[16] M. Blunt, D. H. Fenwick, and D. Zhou, in *Proceedings of the 9th SPE/DOE Symposium on Improved Oil Recovery, Tulsa* (SPE, Richardson, 1994).
[17] R. Lenormand, C. Zarcone, and A. Sarr, J. Fluid Mech. **135**, 337 (1983).
[18] M. Blunt and P. King, Transp. Porous Media **6**, 407 (1991).
[19] M. Blunt, M. J. King, and H. Scher, Phys. Rev. A **46**, 7680 (1992); M. Blunt and H. Scher, Phys. Rev. E **52**, 6387 (1995).
[20] G. R. Jerauld and S. J. Salter, Transp. Porous Media **5**, 102 (1990).
[21] A. A. Heiba, H. T. Davis, and L. E. Scriven, in *Proceedings of the 4th SPE/DOE Symposium on Enhanced Oil Recovery, Tulsa* (SPE, Richardson, 1984).
[22] D. H. Fenwick and M. Blunt (unpublished).
[23] W. E. Soll and A. Celia, Adv. Water Resour. **16**, 107 (1993).
[24] A. W. Adamson, *Physical Chemistry of Surfaces* (Wiley, New York, 1990).
[25] G. J. Hirasaki, J. Adhes. Sci. Technol. **7**, 285 (1993).
[26] M. Dong, F. A. L. Dullien, and I. Chatzis, J. Colloid Interface Sci. **172**, 21 (1995).
[27] R. Lenormand, E. Touboul, and C. Zarcone, J. Fluid Mech. **189**, 165 (1988).
[28] L. Colgan, in *Computational Techniques for Differential Equations*, edited by J. Noye (Elsevier, Amsterdam, 1984).
[29] D. E. Dria, G. A. Pope, and K. Sepehrnoori, in *Proceedings of the 7th SPE/DOE Symposium on Enhanced Oil Recovery, Tulsa* (SPE, Richardson, 1990).